J Appl Electrochem (2009) 39:913–920
DOI 10.1007/s10800-008-9739-4

ORIGINAL PAPER

Influence of heat treatment and microstructure on the corrosion of magnesium alloy Mg-10Gd-3Y-0.4Zr

Li-Ming Peng · Jian-Wei Chang · Xing-Wu Guo · Andrej Atrens · Wen-Jiang Ding · Ying-Hong Peng

Received: 23 July 2008 / Accepted: 24 November 2008 / Published online: 13 December 2008

Abstract The corrosion of Mg alloy Mg-10Gd-3Y-0.4Zr, in the as-cast (F), solution treated (T4) and aged (T6) conditions, was investigated in 5% NaCl solution by immersion tests and potentiodynamic polarization measurements. The as-cast (F) condition had the highest corrosion rate due to micro-galvanic corrosion of the α-Mg matrix by the eutectic. Solution treatment led to the lowest corrosion rate, attributed to the absence of any second phase and a relatively compact protective surface film. Ageing at 250 °C increased the corrosion rate with increasing ageing time to 193 h attributed to increasing micro-galvanic corrosion acceleration of the Mg matrix by increasing amounts of the precipitates. Ageing for longer periods caused a decrease in the corrosion rate attributed to some barrier effect by a nearly continuous second-phase network. Electrochemical measurements did not give accurate evaluation of the corrosion rate in agreement with the immersion tests.

Keywords Corrosion · Heat treatment · Mg-Gd-Y-Zr alloy · Microstructure · Potentiodynamic polarization curve

L.-M. Peng · J.-W. Chang · X.-W. Guo · W.-J. Ding
National Engineering Research Center of Light Alloys Net Forming (LAF), School of Materials Science and Engineering, Shanghai Jiao Tong University, 800 Dong chuan Road, Shanghai 200240, China

J.-W. Chang (✉) · Y.-H. Peng
School of Mechanical Engineering, Shanghai Jiao Tong University, 800 Dong chuan Road, Shanghai 200240, China
e-mail: changpp652@163.com

A. Atrens
Division of Materials, School of Engineering, The University of Queensland, Brisbane, QLD 4072, Australia

1 Introduction

Precipitation-hardening magnesium-rare earth (Mg-RE) alloys are attractive for aerospace and automotive applications because of their high specific strength and good creep resistance [1]. There is a significant body of research on the precipitation reaction [2–4]. Recent work on Mg-Gd-Y [5], Mg-Gd-Nd [6], Mg-Dy-Nd and Mg-Y-Nd [7, 8] has detailed the four stage precipitation sequence, SSSS → $\beta''(DO_{19})$ → β'(cbco) → β_1(fcc) → β(fcc), from the supersaturated solid solution (SSSS) to the equilibrium precipitate, β(fcc), via the intermediate meta-stable precipitates, $\beta''(DO_{19})$, β'(cbco) and β_1(fcc). These microstructure changes result in a typical precipitation hardening response.

The influence of microstructure on the corrosion mechanism of Mg alloys has been elucidated by prior research mainly focused on Mg-Al alloys [9–21]. Second phases, in multi-phase Mg alloys, have three effects: (i) the second phase has the tendency to accelerate the corrosion of the matrix (α-Mg) and so a multi-phase alloy has typically a corrosion rate higher than that of high purity Mg [9, 10], (ii) the second phase can cause a barrier effect if the second phase is finely divided and essentially continuous as occurs in some cases at the surface of die-castings [12] (the skin effect) and (iii) a continuous second phase along grain or dendrite boundaries (as in many creep resistant alloys) leads to intergranular stress corrosion cracking (because of micro-galvanic corrosion of the adjacent α phase) [14, 15]. Are the corrosion mechanisms the same in other Mg-alloy systems? Recent research did, in fact, show that the same mechanisms were important for the corrosion of ZE41 [22, 23]. What about the influence of nano-scale second phase particles in precipitation-hardening alloys? This point is addressed in the present investigation on the corrosion behaviour of Mg-10Gd-3Y-0.4Zr (GW103K) as influenced

by microstructure; heat treatment conditions studied were the as-cast (F), solution treated (T4) and aged (at 250 °C) (T6), investigated using immersion test and electrochemical measurement.

2 Experimental

2.1 Material

An ingot, with a nominal composition Mg-10Gd-3Y-0.4Zr (GW103K), was prepared by melting high-purity Mg (99.95%) together with appropriate quantities of Mg-25wt%Gd, Mg-25wt%Y and Mg-30wt%Zr master alloys, in an electric resistance furnace, under a protective atmosphere of CO_2 and SF_6 with the volume ratio of 100:1. Table 1 presents the actual chemical composition of the alloy as determined by inductively coupled plasma atomic emission spectroscopy (ICP-AES). Solution treatment (T4) was 6 h at 500 °C in an argon atmosphere followed by quenching into hot water at ~80 °C. Solution treated specimens were aged (T6) in an oil bath at 250 °C for 0.5, 16, 193 and 500 h. Vickers hardness measurements used a 49 N load and a holding time of 15 s. The specimens for immersion test were discs, 5 mm in thickness, 1,884 mm^2 surface area. Each specimen was suspended, in the test solution during the immersion test, using a plastic string through a hole, 2.5 mm in diameter near one edge of the specimen.

The microstructure was recorded using optical microscopy (OM). Scanning electron microscopy (SEM) was used to study the appearance of the corrosion products and the corroded surfaces after removal of the corrosion products.

2.2 Immersion test

The corrosion rate was measured using three or four replicate specimens, for each microstructure condition, immersed for 3 days at 25 ± 2 °C in 5 wt% NaCl aqueous solution, prepared with AR grade NaCl and distilled water. Each specimen was polished successively on 320 grit waterproof abrasive paper and 3 grit metallographic paper, washed with distilled water, dried in warm flowing air and weighed to determine the original weight. During the first few hours of immersion, the solution pH increased from neutral to pH ~11 due to the precipitation of $Mg(OH)_2$ because of its low solubility. Thereafter the pH remained constant at ~11. Because the time of the initial increase in pH was short (a few hours) compared with the test duration (3 days), the corrosion rates measured were essentially the same as measured in a solution saturated with $Mg(OH)_2$. After the immersion test, each specimen was washed with distilled water and dried. One sample was used for the corrosion product analysis. The other samples were used to determine the corrosion rate by means of the metal weight loss. The corrosion products were removed by sample immersion in a solution of 200 g L^{-1} CrO_3 + 10 g L^{-1} $AgNO_3$ at ambient temperature for 7 min. Separate experiments demonstrated that this treatment removes all the corrosion products without removing any Mg metal. Each specimen was then washed with distilled water, dried in the warm flowing air and weighed to determine the weight after corrosion. The corrosion rate was reported as (i) the weight loss rate, ΔW, (i.e. the decrease in metal weight divided by the immersion time and surface area [mg cm^{-2} d^{-1}]) and (ii) the equivalent penetration rate, $P_{\Delta W}$/mm^{-1} $year^{-1}$.The penetration rate was related to the weight loss rate, ΔW, using the following conversion [13, 21, 22, 24–26]:

$$P_{\Delta W}/\text{mm year}^{-1} = 2.10\Delta W/\text{mg cm}^{-2}\text{d}^{-1}. \quad (1)$$

Table 1 Chemical compositions of GWK103K/wt%

Alloy	Gd	Y	Zr	Fe	Ni	Mg
GW103K	9.93	2.85	0.4	<0.002	<0.002	Balance

2.3 Potentiodynamic polarization curves

Potentiodynamic polarization curves were measured with metallographic polished specimens in 5% NaCl solution saturated with $Mg(OH)_2$ that gave a stable pH of ~11, using a three-electrode electrochemical cell and a scanning rate of 1 mV s^{-1}. The reference electrode was a saturated calomel electrode (SCE); the counter electrode was a high-density graphite electrode. After immersion for 1 h, the polarization was started from a potential of −250 mV (cathodic) relative to the open circuit potential and was stopped at an anodic potential where the anodic current increased dramatically. At least two tests were conducted for each microstructure condition; these confirmed the reproducibility of the polarization curves. Polarisation curves were used to gain a measure of the corrosion rate, I_{corr}, by Tafel extrapolation of the cathodic branch and the corrosion potential, E_{corr}. The corrosion current density (I_{corr}/mA cm^{-2}) is related [13, 21–24] to the average penetration rate using:

$$P_I = 22.85\ I_{corr}. \quad (2)$$

3 Results

3.1 Age hardening and microstructure

Figure 1 shows (i) the age hardening curve for GW103K aged at 250 °C and (ii) TEM micrographs of the

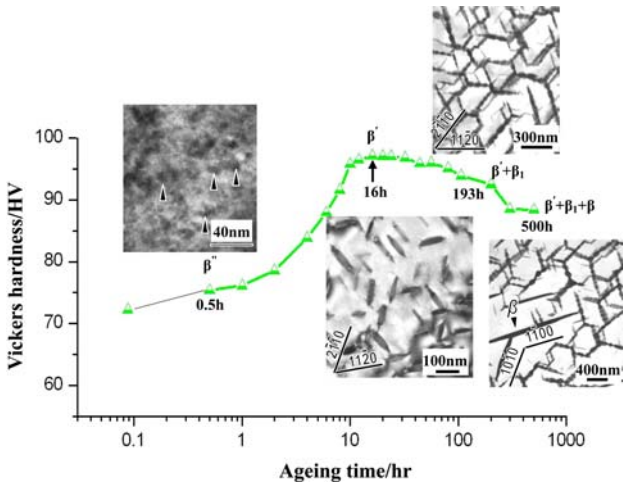

Fig. 1 An age hardening curve at 250 °C for Mg-10Gd-3Y-0.4Zr and TEM micrographs of the precipitates

precipitates [5]. The hardness increased rapidly after ~1 h, the peak hardness occurred at ~16 h, there was a plateau from 10 to 60 h and further ageing led to a slow decrease in hardness. Corrosion was studied for ageing times of 0.5, 16, 193 and 500 h, which corresponded to under-aged, peak-aged, slightly over-aged and significantly over-aged conditions. The precipitates, after ageing 0.5 h (T6-0.5 h), were mainly meta-stable β''. The peak-aged (T6-16 h) condition contained predominantly meta-stable β' phase. The over-aged conditions (193 and 500 h) contained β' and β_1, with a minor fraction of β phase for 500 h ageing.

Figure 2 presents optical micrographs of GW103K in the as-cast (F), solution treated (T4) and aged (T6-193 h) conditions. The as-cast (F) microstructure consisted of the Mg matrix and the eutectic, distributed along the dendrite boundaries, especially at the triple points (Fig. 2a). The solution treated (T4) microstructure was single grained α-Mg; the Gd and Y in the eutectic had dissolved in the Mg-matrix (Fig. 2b). Optical microscopy did not reveal any change in microstructure between the solution treated (T4) condition and the microstructure after ageing 0.5 h (T6-0.5 h). However, precipitates were visible after ageing 16 h or longer; the optical micrographs were similar after ageing at 16, 193 and 500 h. Figure 2c shows a typical optical micrograph of the alloy aged 193 h (T6-193 h): there were small cuboid-shaped phases distributed unevenly in the matrix and boundaries and Zr-rich cores in the centre of most grains. The GW103K microstructures were similar to those of NZ30K [27].

3.2 Immersion test

Figure 3 presents the corrosion rates for GW103K in the different heat treatment conditions, measured by immersion in 5% NaCl solution for 3 days. GW103K in the as-cast condition (F) showed the highest corrosion rate, whilst GW103K in the solution treated condition (T4) showed the lowest corrosion rate. The corrosion rates in the aged (T6) conditions increased with increasing ageing time from 0.5 to 193 h and then decreased from 193 to 500 h.

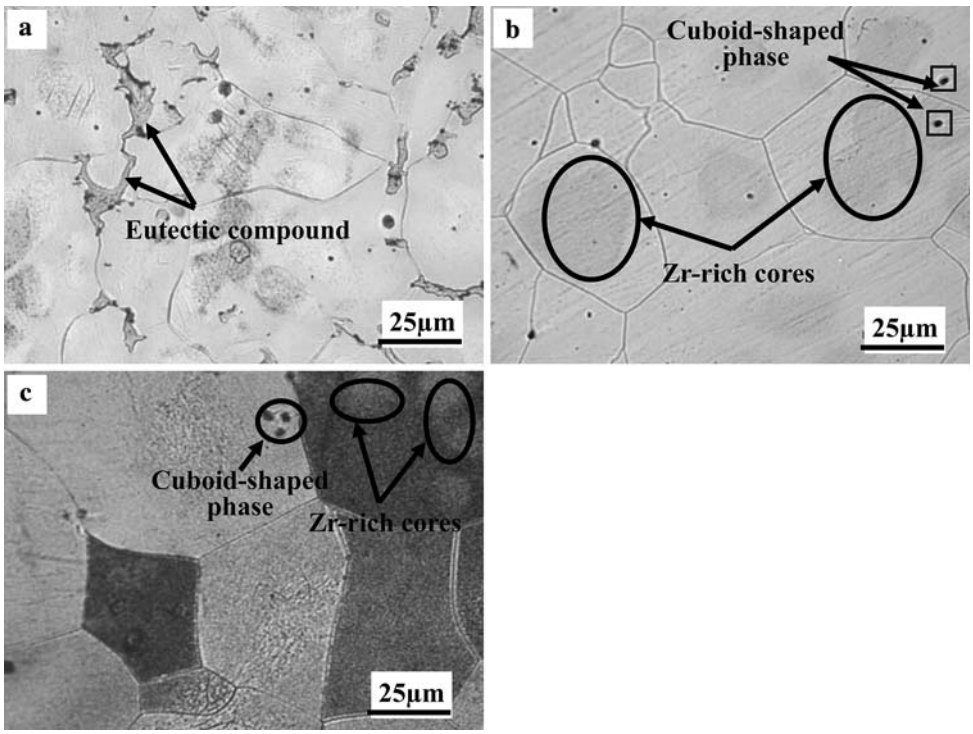

Fig. 2 Optical micrograph of GW103K: **a** as-cast (F), **b** solution treated (T4) and **c** aged 193 h (T6-193 h)

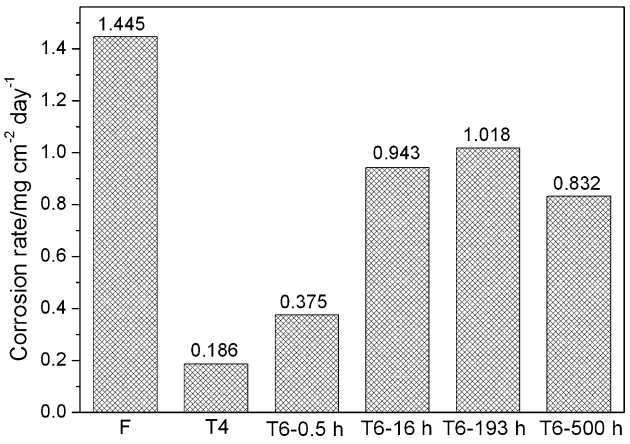

Fig. 3 Corrosion rates of GW103K measured by immersion in 5% NaCl solution for 3 days

The alloy aged at 193 h (T6-193 h) showed the highest corrosion rate for the aged alloys.

Figure 4 presents the macroscopic surface appearance of the corroded specimens. The as-cast condition (F) and the slightly over-aged condition (T6-196 h) had areas of significant localized corrosion, which appeared as areas covered with loose white corrosion products. In contrast, the other three conditions exhibited general corrosion. The visual severity of corrosion was in agreement with the corrosion rates in Fig. 3.

Figure 5 shows the micro-morphologies of the corroded surface of the specimens after immersion in 5% NaCl solution for 3 days and removal of the corrosion products. Figure 5a shows that severe micro-galvanic corrosion had occurred in the matrix next to the eutectic micro-constituent in the as-cast condition (F). Figure 5b shows (i) a small degree of corrosion and (ii) that the corrosion morphology was general corrosion with negligible localized corrosion for the solution treated (T4) condition, attributed to dissolution of the Gd, Y in solid solution in the Mg-matrix from the eutectic micro-constituent. The corrosion morphology after ageing 0.5 h (T6-0.5 h) was similar to that of the solution treated condition (T4). The degree of corrosion increased after ageing 16 h (T6-16 h). The corrosion morphology was similar for ageing at 16, 193 and 500 h. Figure 5c shows that the corrosion of the Zr-rich cores in the centre of the grains was smaller than that of the adjacent Zr-poor regions at the edge of the grains. Corrosion initiated in the Zr-poor regions and spread across the Zr-rich cores. There was little corrosion of cuboid-shaped phases but significant corrosion of the adjacent α-Mg matrix (Fig. 5d).

3.3 Corrosion products

The areas of non-localized-corrosion of the specimens after the immersion test (Fig. 4), examined using SEM, Fig. 6, indicated that the corrosion products, in each case, were composed of tiny erect flakes aligned perpendicular to the alloy surface. The phase composition of these corrosion products was previously [28] identified by X-ray diffraction to be mainly $Mg(OH)_2$ with a small amount of $Gd(OH)_3$. The cross sections indicate that the corrosion product films on F and T4 specimens (Fig. 6a′, b′) were relatively compact, whereas the corrosion product films were looser on the specimens aged 16 to 500 h (T6-16 h, Fig. 6c′ and T6-500 h, Fig. 6d′). The thickness of the

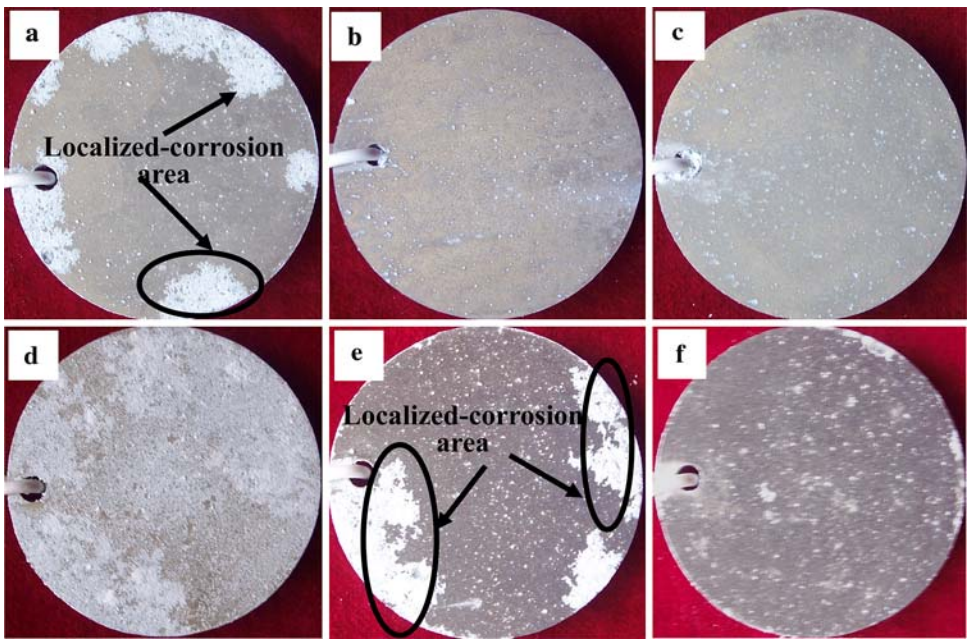

Fig. 4 Macro-appearance of corroded surfaces of GW103K after immersion in 5% NaCl solution for 3 days **a** as-cast (F), **b** solution treated (T4), **c** aged 0.5 h (T6-0.5 h), **d** aged 16 h (T6-16 h), **e** aged 193 h (T6-193 h) and **f** aged 500 h (T6-500 h)

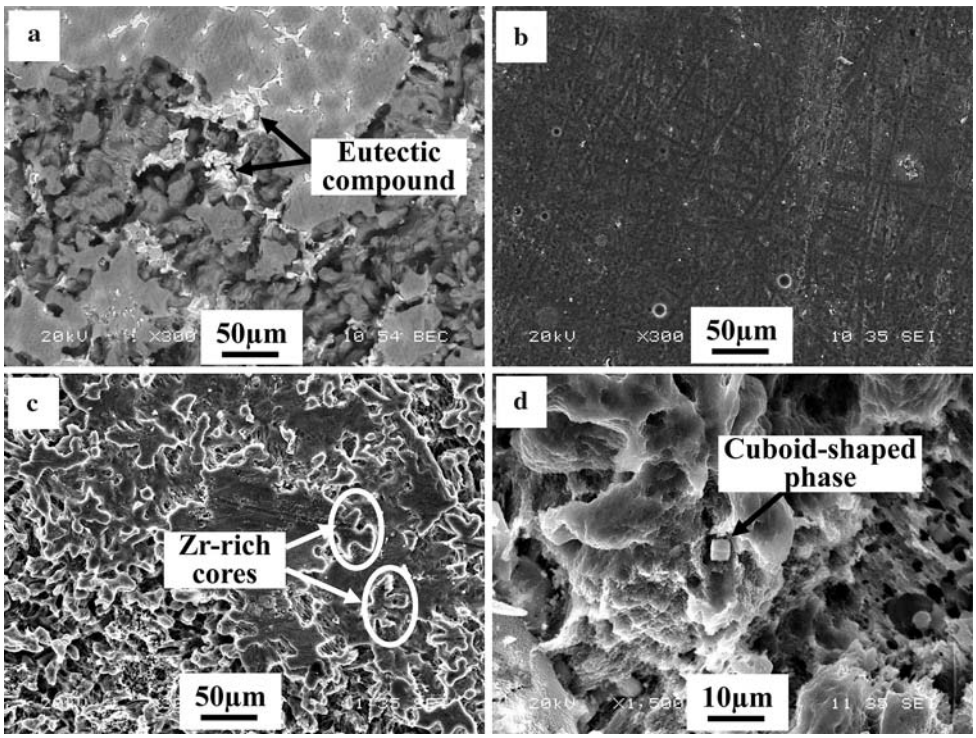

Fig. 5 Micro-appearance (SEM images) of the corroded surfaces after immersion in 5% NaCl solution for 3 days and after removal of the corrosion products: **a** back scattered electron image of as-cast (F) condition, **b** secondary electron image of solution treated (T4) condition, **c** secondary electron image of condition aged for 16 h (T6-16 h) and **d** secondary electron image of condition aged for 193 h (T6-193 h)

corrosion product film was ~3 μm in the as-cast (F) and solution treated (T4) conditions, ~15 μm in the peak-aged condition (T6-16 h) and ~5 μm in the significantly over-aged condition (T6-500 h). The peak-aged condition (T6-16 h) had the thickest corrosion product film. The solution treated condition (T4) had a compact corrosion product film; this correlated with the low corrosion rate and may be the explanation for the low corrosion rate. The as-cast condition (F) also had a compact corrosion product film; its higher corrosion rate was attributed to the micro-galvanic acceleration of the corrosion of the α-Mg adjacent to the eutectic micro-constituent.

3.4 Potentiodynamic polarization curves

Figure 7 presents the potentiodynamic polarization curves measured in 5% NaCl solution saturated with $Mg(OH)_2$, for the specimens after immersion for 1 h in the solution. Before measurement of each potentiodynamic polarization curve, the open circuit potential of the specimen was comparatively stable, a corrosion product film had formed on the surface of the specimens and no clear localized corrosion had occurred.

Table 2 presents values of I_{corr}, P_I, E_{corr} and β_c values for GW103K in the as-cast (F), solution treated (T4) and aged (T6) conditions, evaluated from polarisation curves measured in 5% NaCl solution saturated with $Mg(OH)_2$. Also listed for comparison are $P_{\Delta W}$ and $P_{\Delta W}/P_I$. The cathodic Tafel slope was similar for all conditions, indicating similar electrochemical reactions for hydrogen evolution. The values of I_{corr}, and the corresponding corrosion penetration rate, P_I, for the different microstructure conditions correlated with the corrosion rates measured from weight loss, $P_{\Delta W}$, but did not agree in magnitude. Moreover the ratio $P_{\Delta W}/P_I$ was not constant, indicating that the electrochemical method based on Tafel extrapolation of the cathodic polarisation curve does not provide a good measurement of the corrosion rate. This is in agreement with prior research [10, 11, 21, 25, 29, 30].

The polarization curves indicated that the as-cast condition (F) had the most positive corrosion potential and the solid solution condition (T4) had the most negative corrosion potential, whereas the corrosion potentials of the aged conditions (T6-16 h and T6-500 h) were almost the same and were between those of the as-cast (F) and solid solution (T4) conditions.

The positive corrosion potential in the as-cast condition (F) was attributed to the presence of the second phase at the dendrite boundaries, because the potential of an alloy was determined by the potential of the constituent phases and the area fraction covered by each phase [31]. Figure 5a showed that the eutectic was still intact in the corroded area in the as-cast (F) condition. This indicated that the corrosion potential of the eutectic was more positive than that of the α phase and shifted the corrosion potential of the alloy towards more positive values. The solution treated (T4) condition had a more negative potential because of the dissolution of the rare earth elements (Gd and Y) of the

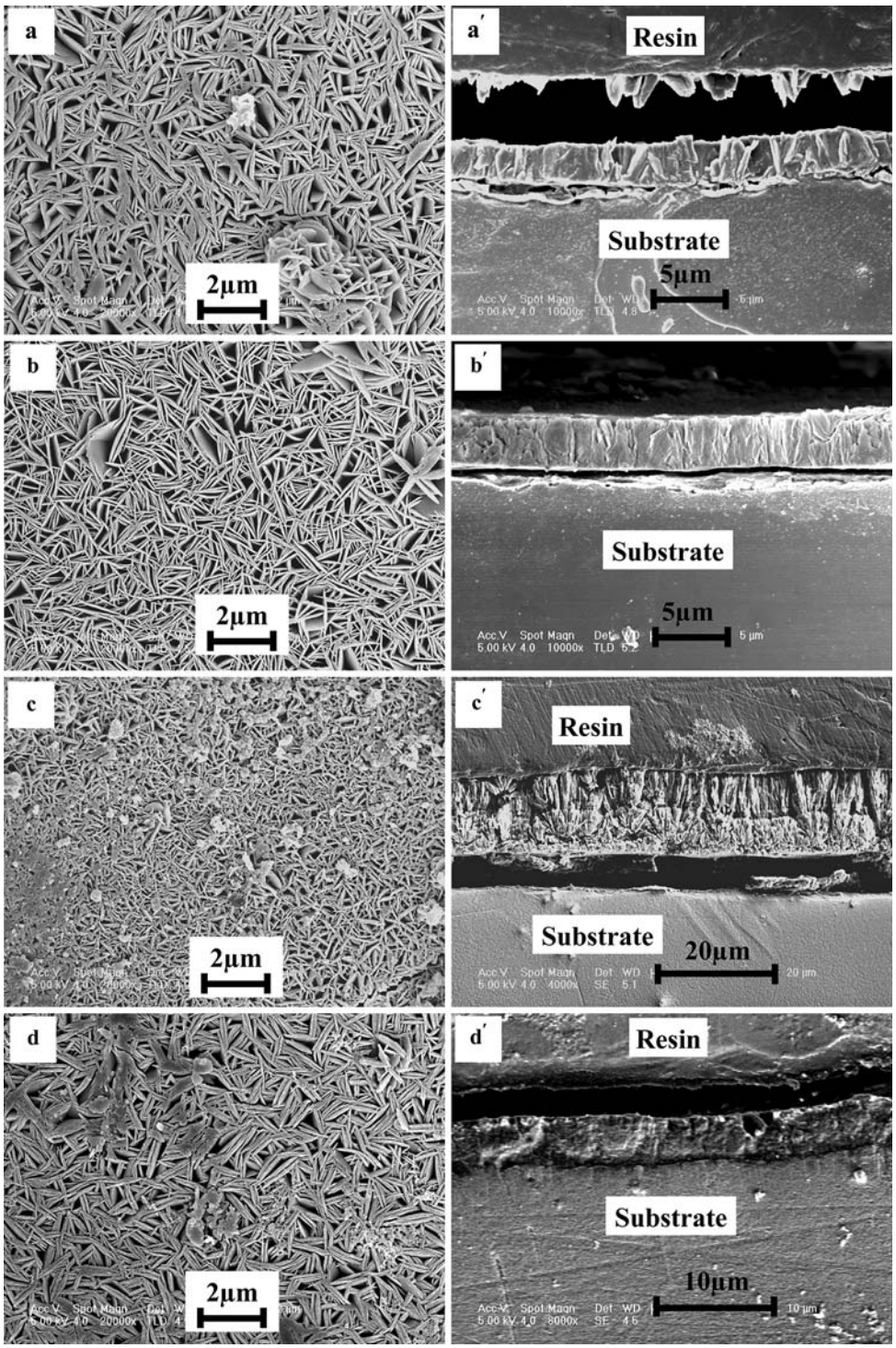

Fig. 6 Surface (left) and cross section (right) SEM images of the corrosion product layer on GW103K after immersion in 5% NaCl solution for 3 days: **a**, **a′** as-cast (F), **b**, **b′** solution treated (T4), **c**, **c′** aged for 16 h (T6-16 h) and **d**, **d′** aged for 500 h (T6-500 h)

eutectic into the Mg-matrix. In the aged condition, the amount of the precipitates (β' and β_1) increased with ageing time and the corrosion potential was accordingly increased to more positive values.

The cathodic polarization curves were associated with hydrogen evolution and the anodic curves represented the dissolution of magnesium [9, 10]. The cathodic current density for the solution treated condition (T4) was lower than that of the other conditions, indicating that hydrogen evolution was most difficult on this surface, which was attributed to the absence of second phase. The anodic curve for the 500 h aged condition (T6-500 h) had a region of slowly increasing current followed by a rapid increase with increasing potential. The region of slowly increasing

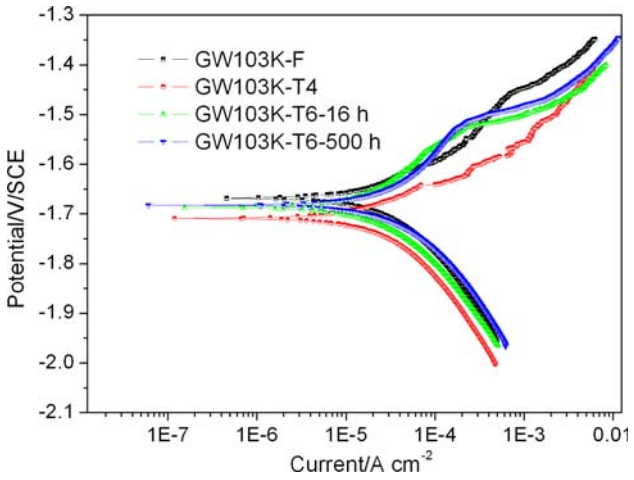

Fig. 7 Polarization curves of GW103K after immersion in 5% NaCl solution saturated with Mg $(OH)_2$ for 1 h

Table 2 I_{corr}, P_I, E_{corr} and β_c values for GW103K in the F, T4 and T6 conditions, evaluated from polarisation curves measured in 5% NaCl saturated with $Mg(OH)_2$

Material	I_{corr} (μA cm^{-2})	P_I (mm $year^{-1}$)	E_{corr}/V/ SCE	β_c/V/ SCE	$P_{\Delta W}$ (mm $year^{-1}$)	$P_{\Delta W}/P_I$
GW103K-F	50	1.1	−1.67	0.23	3.00	2.70
GW103K-T4	24	0.54	−1.71	0.17	0.39	0.71
GW103K-T6-16 h	31	0.71	−1.69	0.20	2.00	2.80
GW103K-T6-500 h	30	0.67	−1.68	0.19	1.70	2.60

Also listed for comparison are $P_{\Delta W}$ and $P_{\Delta W}/P_I$

current was attributed to the presence of the continuous network of interconnected precipitates (β', β_1 and β).

4 Discussion

The difference in corrosion rates of GW103K in different heat treatment conditions was related to the microstructure. Figure 2a shows that the as-cast condition (F) was composed of the matrix and the (Gd + Y)-containing eutectic, whereas the solution treated (T4) condition consisted of single α-Mg phase (Fig. 2b). Figure 5a shows that there was micro-galvanic acceleration of the corrosion of the α-Mg by the eutectic. Therefore the high corrosion rate of the as-cast (F) condition was attributed to the eutectic. In contrast, in the solution treated (T4) condition all the (Gd + Y)-rich eutectic had dissolved into the Mg matrix, so there was a high concentration of the rare earth elements (Gd and Y) in the α-Mg and as a result the corrosion rate was low in agreement with our prior study [27] and that of Krishnamurthy et al. [32].

The increase of the corrosion rates with increasing ageing time up to 193 h, which correlated with an increasing volume fraction of second phase, was consistent with the prior studies on AZ91D and ZE41 [12, 13, 21, 22]. The increase of corrosion rate for GW103K with ageing time to 193 h indicated that the precipitates (β'', β' and β_1) also acted as efficient cathodes and caused micro-galvanic corrosion. After ageing for 500 h, owing to the formation of nearly continuous precipitates (β', β_1 and β) network, the corrosion rate decreased. This indicated that the arrangement of the coarse β phase acted as a corrosion barrier to some degree in agreement with Kiryuu et al. [33], who also found the over-aged Mg-10Gd-3Nd-Zr (wt%) and Mg-10Dy-3Nd-Zr (wt%) alloys had lower corrosion rates.

5 Conclusions

(1) Heat treatment and microstructure influenced the corrosion of GW103K as for other Mg alloys AZ91 and ZE41.
(2) The as-cast condition had the highest corrosion rate due to the micro-galvanic corrosion of the α-Mg matrix by the eutectic. Solution treatment led to the lowest corrosion rate, attributed to the absence of any second phase and a relatively compact protective surface film. Ageing at 250 °C increased the corrosion rate with increasing ageing time to 193 h attributed to increasing micro-galvanic corrosion acceleration of the Mg matrix by increasing amounts of the precipitates. Ageing for longer periods caused a decrease in the corrosion rate attributed to some barrier effect by a nearly continuous β-network.
(3) Electrochemical measurements did not give accurate evaluation of the corrosion rate in agreement with prior studies

Acknowledgements This work was supported by Postdoctoral foundation of China (No. 20080430657), Program of Shanghai Subject Chief Scientist of China (No. 08XD14020) and National Basic Research Program of China (No. 2007CB613701). The authors would like to thank Dr. Yi-jian Lai of the Center of Analysis and Measurement of Shanghai Jiao Tong University for his help in observation of the corrosion products with Field Emission Scanning Electron Microscope (FE-SEM).

References

1. Rokhlin LL (2003) Magnesium alloys containing rare earth metals. Taylor and Francis, London
2. Lorimer GW (1986) Proceedings of magnesium technology. Institute of Metals, London
3. Smola B, Stuliikovai I, Von Buch F, Mordike BL (2002) Mater Sci Eng A 324:113
4. Vostryi P, Smola B, Stuliikovai I, Von Buch F, Mordike BL (1999) Phys Stat Sol A 175:491

5. He SM, Zeng XQ, Peng LM, Gao X, Nie JF, Ding WJ (2006) J Alloys Comp 421:309
6. Apps PJ, Karimzadeh H, King JF, Lorimer GW (2003) Scr Mater 48:1023
7. Nie JF, Muddle BC (2000) Acta Mater 48:1691
8. Antion C, Donnadieu P, Perrard F, Deschamps A, Tassin C, Pisch A (2003) Acta Mater 51:5335
9. Song G, Atrens A (1999) Adv Eng Mater 1:11
10. Song G, Atrens A (2003) Adv Eng Mater 5:837
11. Song G, Atrens A (2007) Adv Eng Mater 9:177
12. Song G, Atrens A, Dargusch M (1999) Corros Sci 41:249
13. Zhao MC, Liu M, Song G, Atrens A (2008) Corros Sci 50:1939
14. Zhao MC, Liu M, Song G, Atrens A (2008) Adv Eng Mater 10:93
15. Winzer N, Atrens A, Song G, Ghali E, Dietzel W, Kainer KU, Hort N, Blawert C (2005) Adv Eng Mater 7:659
16. Kannan MB, Dietzel W, Blawert C, Atrens A, Lyon P (2008) Mater Sci Eng A 480:529
17. Aung NN, Zhou W (2002) J Appl Electrochem 32:1397
18. Beldijoudi T, Fiaud C, Robbiola L (1993) Corrosion 8:738
19. Hsiao HY, Tsai WT (2005) J Mater Res 20:2763
20. Song G, Bowles AL, John DH (2004) Mater Sci Eng A 366:74
21. Ambat R, Aung NN, Zhou W (2000) Corros Sci 42:1433
22. Zhao MC, Liu M, Song G, Atrens A (2008) Corros Sci 50:3168
23. Zhao MC, Liu M, Song G, Atrens A (2008) Adv Eng Mater 10:104
24. ASM International (1987) Metals handbook. ASM International, Materials Park
25. Uhlig HH, Revie RW (1985) Corrosion and corrosion control. Wiley, New York
26. Song G, Atrens A, John D (2001) Magnesium technology. Hryn, New Orleans
27. Chang JW, Guo XW, Fu PH, Peng LM, Ding WJ (2007) Electrochim Acta 52:3160
28. Guo XW, Chang JW, He SM, Ding WJ, Wang X (2007) Electrochim Acta 52:2570
29. Scharf C, Ditze A, Shkurankov A, Morales E, Blawert C, Dietzel W, Kainer KU (2005) Adv Eng Mater 7:1134
30. Jia JX, Atrens A, Song G, Muster T (2005) Mater Corros 56:468
31. Mansfeld F (1971) Corrosion 27:436
32. Krishnamurthy S, Khobaib M, Robertson E, Froes FH (1988) Mater Sci Eng 99:507
33. Kiryuu M, Okumura H, Kamado S, Kojima Y, Ninomiya R, Nakatsugawa I (1996) J Jpn Inst Light Met 46:39